

Temperature Dependence of Protein Dynamics: Computer Simulation Analysis of Neutron Scattering Properties

Jennifer A. Hayward and Jeremy C. Smith

Lehrstuhl für Biocomputing, IWR, Universität Heidelberg, D-69120 Heidelberg, Germany

ABSTRACT The temperature dependence of the internal dynamics of an isolated protein, bovine pancreatic trypsin inhibitor, is examined using normal mode analysis and molecular dynamics (MD) simulation. It is found that the protein exhibits marked anharmonic dynamics at temperatures of ~ 100 – 120 K, as evidenced by departure of the MD-derived average mean square displacement from that of the harmonic model. This activation of anharmonic dynamics is at lower temperatures than previously detected in proteins and is found in the absence of solvent molecules. The simulation data are also used to investigate neutron scattering properties. The effects are determined of instrumental energy resolution and of approximations commonly used to extract mean square displacement data from elastic scattering experiments. Both the presence of a distribution of mean square displacements in the protein and the use of the Gaussian approximation to the dynamic structure factor lead to quantified underestimation of the mean square displacement obtained.

INTRODUCTION

The temperature dependence of the internal motion of proteins and its relation to function have been much studied using a variety of experimental and theoretical techniques (e.g., Knapp et al., 1982; Parak and Knapp, 1984; Doster et al., 1989; Smith et al., 1990; Smith, 1991, 2000; Rasmussen et al., 1992; Demmel et al., 1997; Fitter et al., 1997; Cordone et al., 1998; Ostermann et al., 2000). These studies have revealed a smooth change in the slope of the temperature dependence of the average mean square displacement of atoms in proteins, $\langle u^2 \rangle$, in the temperature range ~ 170 – 240 K. At temperatures below this transition, the dynamics appears harmonic and vibrational. Above the transition, anharmonic motions are also present. This change in dynamics resembles that seen in the liquid–glass transition (Angell, 1995). The anharmonic dynamics involve diffusive motion and allow sampling of different conformational sub-states (Elber and Karplus, 1987; Karplus and Petsko, 1990; Frauenfelder et al., 1991; Kneller and Smith, 1994). Some studies have found a correlation between the onset of the anharmonic motion and protein activity (Parak et al., 1980; Rasmussen et al., 1992; Ferrand et al., 1993; Ding et al., 1994; Ostermann et al., 2000).

In the present paper, we use computer simulation to examine two aspects of this temperature dependence. The first concerns the role of solvent. Experimental and computational work has indicated that the activation of anharmonic dynamics is strongly influenced by solvent (Ferrand et al., 1993; Demmel et al., 1997; Fitter et al., 1998a,b; Fitter, 1999; Vitkup et al., 2000; Réat et al., 2000). However, the question as to whether solvent is required for the

activation of anharmonic dynamics is as yet unanswered, i.e., it is not known whether an isolated protein in the absence of solvent would have any transition from harmonic to anharmonic dynamics, or whether it remains harmonic and vibrational up to room temperature. Neutron-scattering experiments on dry protein samples show no clear evidence of dynamical transition behavior (Ferrand et al., 1993; Fitter et al., 1997, 1998b; Lehnert et al., 1998; Fitter, 1999; Réat et al., 2000). However, a definitive answer to this question requires the obtention of a harmonic reference state. Here, molecular dynamics (MD) simulations are performed on a model system, an isolated bovine pancreatic trypsin inhibitor (BPTI) molecule, as a function of temperature. To set a harmonic reference, normal mode analysis (NMA) is performed. In NMA, the harmonic approximation to the potential energy function is made, and the resulting atomic trajectories are a superposition of vibrational normal modes. In contrast, in MD simulations, the full anharmonic potential energy function is used. The temperature dependence of $\langle u^2 \rangle$ is calculated here from both NMA and MD. Deviation of the MD displacements from the NMA results indicates the presence of anharmonic dynamics.

The second question addressed here concerns the relationship between temperature-dependent dynamical quantities in proteins and neutron-scattering measurements. Neutron scattering is a technique of major importance for examining dynamical transition properties and is complementary to MD/NMA, probing similar length and time-scales (Lovesey, 1984; Smith, 1991). Much of the dynamical transition work has involved examination of elastic neutron scattering (e.g., Ferrand et al., 1993; Fitter et al., 1997; Daniel et al., 1998, 1999; Lehnert et al., 1998; Cordone et al., 1999; Dunn et al., 2000; Réat et al., 2000; Zaccai, 2000). Atomic motions lead to a reduction in elastic scattering intensity in a manner closely analogous to that seen in crystallographic Bragg scattering. However, the interpretation of the elastic neutron-scattering data in terms of $\langle u^2 \rangle$ involves approximations in the description of the

Submitted August 1, 2001 and accepted for publication October 3, 2001.

Address reprint requests to Jeremy C. Smith, Lehrstuhl für Biocomputing, IWR, Im Neuenheimer Feld 368, Universität Heidelberg, D-69120 Heidelberg, Germany. Tel.: +49-6221-54-88-57; Fax: +49-6221-54-88-68; E-mail: biocomputing@iwr.uni-heidelberg.de.

© 2002 by the Biophysical Society

0006-3495/02/03/1216/10 \$2.00

dynamics of the atoms in a protein and its relation to scattering amplitudes. In view of the volume of elastic neutron scattering work that has recently appeared, it is now timely to examine the approximations made. Therefore, here we use the MD simulation as a test “experimental data set.” The measurable quantity, the dynamic structure factor, is calculated from the simulation trajectories and then subjected to data analysis similar to that performed experimentally. The effect of the approximations on the derived $\langle u^2 \rangle$ can then be determined by comparison with $\langle u^2 \rangle$ calculated exactly from the MD simulations.

Two approximations in particular are examined. The first of these is the so-called “Gaussian approximation” for the q -dependence of the dynamic structure factor (where q is the scattering vector). Second, the effect of the existence of a distribution of mean square displacements in the protein, rather than one uniform value, is explored. This “motional heterogeneity” leads to an additional non-Gaussian contribution to the dynamic structure factor. Finally, the effect of the instrumental energy resolution on the $\langle u^2 \rangle$ obtained is also probed. It is found that each of these effects reduces the $\langle u^2 \rangle$ obtained—the present calculations provide estimates of how large these effects are and under which experimental conditions they are likely to exert an influence.

METHODS

Molecular dynamics simulations

The model system of BPTI consists of 892 atoms, 58 residues, and 4 internal water molecules. This model system is an approximation of a dry powder sample, as has been used in several neutron experiments (Ferrand et al., 1993; Fitter et al., 1997, 1998b; Lehnert et al., 1998; Fitter, 1999; Réat et al., 2000). To mimic typical experimental conditions, the exchangeable hydrogen atoms were replaced by deuterium, leaving 315 hydrogen atoms.

The system was simulated using CHARMM (Brooks et al., 1983) version 27 with all-atom parameter set 22 (Mackerell et al., 1998). The four internal, structural water molecules were represented by the TIP3P potential (Jorgensen et al., 1983). The simulations were performed in the NVE ensemble. A timestep of 0.002 ps was used with SHAKE (Ryckaert et al., 1977) applied to constrain bonds containing hydrogen or deuterium atoms. Nonbonded and electrostatic interactions were truncated using the shifting function (Steinbach and Brooks, 1994) at 13.0 Å and the dielectric constant was set to ϵ_0 .

Simulations were performed at 19 different temperatures: 80, 100, 120, 140 K, then in steps of 10 K to 280 K, and, finally 300 K. The starting structure for the first temperature simulated, 80 K, was the energy-minimized BPTI crystal structure (Parkin et al., 1996) Protein Data Bank reference (1BPI) (Berman et al., 2000). The starting structures for the rest of the simulations at increasing temperatures were the final structures from the preceding temperature. The systems at each temperature were equilibrated for 50 ps and then data collected every 0.1 ps for 2000 ps, i.e., a total simulation time of 2050 ps per temperature. The total simulation time was 38.95 ns, requiring 209 CPU hours running in parallel on 64 processors on an IBM SP2 computer, i.e., 13,376 CPU hours. After the final simulation at 300 K the root mean square deviation of the backbone heavy atoms from the crystal structure was 2 Å, and that calculated using the secondary structural elements only was within 1 Å of the crystal structure.

Normal modes

Normal modes were computed using the VIBRAN module of CHARMM using the same model system and potential function as for the MD simulations. At low temperatures, proteins are trapped in multiple minima leading to structural inhomogeneity (Elber and Karplus, 1987; Frauenfelder et al., 1991; Ostermann et al., 2000). This leads to dynamical inhomogeneity reflected in broadening of theoretical neutron and infrared spectra (Lamy et al., 1996). To take this inhomogeneity into account, 20 structures were taken from the 300-K simulation trajectories at regular intervals and were energy minimized to a root mean square energy gradient of $<10^{-7}$ kcal mol $^{-1}$ Å $^{-1}$. Normal modes were computed in each minimum.

The eigenvalues and eigenvectors from the 20 normal-mode analyses were used to calculate the mean square displacements. Both classical and quantum mechanical mean square displacements were calculated and compared. The classical mean square displacements were calculated and compared. The classical mean square displacement averaged over the atoms in the protein, $\langle u^2 \rangle_{\text{class}}$, is given by

$$\langle u^2 \rangle_{\text{class}} = \frac{2}{N_{\text{atom}}} \sum_{\alpha=1}^{N_{\text{atom}}} \sum_{k=1}^{3N_{\text{atom}}-6} (|\tilde{c}_{\alpha}^k|)^2 \left(\frac{k_B T}{m_{\alpha} \nu_k^2} \right)^2, \quad (1)$$

where N_{atom} is the number of atoms, \tilde{c}_{α}^k is the eigenvector for atom α in mode k , k_B is the Boltzmann constant, T is the temperature, m_{α} is the atomic mass, and ν_k is the mode eigenvalue, or frequency. The equivalent quantum mechanical expression is

$$\langle u^2 \rangle_{\text{qm}} = \frac{2}{N_{\text{atom}}} \sum_{\alpha=1}^{N_{\text{atom}}} \sum_{k=1}^{3N_{\text{atom}}-6} (|\tilde{c}_{\alpha}^k|)^2 \times \left[\frac{\hbar}{2m_{\alpha} \nu_k} \coth \left(\frac{\hbar \nu_k}{2k_B T} \right) \right]^2 \quad (2)$$

where $\hbar = h/2\pi$ and h is the Planck constant.

Neutron-scattering properties

The nMOLDYN package (Kneller et al., 1995) was used to calculate neutron-scattering properties from the MD trajectories.

Dynamic structure factor

The basic measured quantity in inelastic neutron-scattering experiments is the double differential cross section, $d^2\sigma/d\Omega dE$ which is the number of neutrons scattered into the solid angle interval $[\Omega, \Omega + d\Omega]$ and energy interval $[E, E + dE]$, normalized to $d\Omega$, dE , and the flux of the incoming neutrons,

$$\frac{d^2\sigma}{d\Omega dE} = N_{\text{atom}} \frac{k}{k_0} S(\vec{q}, \omega). \quad (3)$$

The quantity $S(\vec{q}, \omega)$ is the dynamic structure factor, and k_0 and k are the moduli of the wave vectors of the incident and scattered neutrons, respectively. These are related to the corresponding neutron energies by $E_0 = \hbar^2 k_0^2 / 2m$ and $E = \hbar^2 k^2 / 2m$ where m is the neutron mass. The energy, ω , and momentum transfer, \vec{q} , in units of \hbar , are given by $\omega = (E_0 - E)/\hbar$ and $\vec{q} = (\vec{k}_0 - \vec{k})/\hbar$. The modulus of the momentum transfer, q , is related to the energy transfer and the scattering angle Θ by

$$q = k_0 \sqrt{2 - \frac{\hbar\omega}{E_0} - 2\sqrt{1 - \frac{\hbar\omega}{E_0}} \cos(\Theta)}. \quad (4)$$

The dynamic structure factor $S(\vec{q}, \omega)$ contains information about the dynamics of the sample. It contains a coherent part arising from self- and

cross-correlations of atomic motions and an incoherent part describing only single atom motions,

$$S_{\text{coh}}(\vec{q}, \omega) = \frac{1}{2\pi} \int_{-\infty}^{+\infty} dt e^{-i\omega t} F_{\text{coh}}(\vec{q}, t), \quad (5)$$

$$F_{\text{coh}}(\vec{q}, t) = \frac{1}{N_{\text{atom}}} \sum_{\alpha, \beta} b_{\alpha, \text{coh}}^* b_{\beta, \text{coh}} \langle e^{-i\vec{q} \cdot \vec{R}_{\alpha}(0)} e^{i\vec{q} \cdot \vec{R}_{\beta}(t)} \rangle, \quad (6)$$

$$S_{\text{inc}}(\vec{q}, \omega) = \frac{1}{2\pi} \int_{-\infty}^{+\infty} dt e^{-i\omega t} F_{\text{inc}}(\vec{q}, t) \quad (7)$$

$$F_{\text{inc}}(\vec{q}, t) = \frac{1}{N_{\text{atom}}} \sum_{\alpha} b_{\alpha, \text{inc}}^2 \langle e^{-i\vec{q} \cdot \vec{R}_{\alpha}(0)} e^{i\vec{q} \cdot \vec{R}_{\alpha}(t)} \rangle. \quad (8)$$

Eqs. 5 and 7 show that the coherent and incoherent dynamic structure factors are time Fourier transforms of the coherent and incoherent intermediate scattering functions, $F_{\text{coh}}(\vec{q}, t)$ and $F_{\text{inc}}(\vec{q}, t)$, respectively. α, β label individual atoms whose positions are specified by their time-dependent position vector operators $\vec{R}_{\alpha}(t)$ and $\vec{R}_{\beta}(t)$ respectively. Each atom has a coherent scattering length $b_{\alpha, \text{coh}}$ and an incoherent scattering length $b_{\alpha, \text{inc}}$ which defines the strength of the interaction between the nucleus of the atom and the neutron. These quantities depend only on the isotope involved. In the present model system, the coherent scattering contribution is very small and the hydrogen atom incoherent scattering dominates ($\sigma_{\text{H, inc}} = 4\pi b_{\text{H, inc}}^2 = 81.67 \times 10^{-24} \text{ cm}^2$). The present results were found to be close to identical whether the nonhydrogen atom scattering was included or not.

The intermediate scattering functions are quantum-mechanical time-correlation functions that are replaced by classical time-correlation functions if they are calculated from MD simulations. The detailed balance condition,

$$S(\vec{q}, \omega) = e^{\beta\hbar\omega} S(-\vec{q}, -\omega), \quad (9)$$

does not hold in the classical limit $\hbar \rightarrow 0$. To take account of this, we assume the semiclassical correction (Lovesey, 1984), given here for isotropic systems, such as the powder under consideration,

$$S(q, \omega) \approx \frac{\beta\hbar\omega}{1 - e^{-\beta\hbar\omega}} S_{\text{cl}}(q, \omega). \quad (10)$$

The shorthand β stands for $1/k_{\text{B}}T$ and $S_{\text{cl}}(q, \omega)$ is the classical dynamic structure factor. The semiclassical correction, Eq. 10, is an approximation valid only in the linear response regime $\hbar\omega < k_{\text{B}}T$.

In the present work, $S(\vec{q}, \omega)$, computed using Eqs. 7–9, was convoluted with the Gaussian-shaped instrumental energy-resolution function of typical neutron spectrometers. Two resolutions were used, corresponding to 100 and 20 μeV (full width at half maximum). These correspond to resolutions that can be obtained using neutron spectrometers commonly used for protein studies.

Gaussian approximation

We test here two approximations commonly used in neutron-scattering data analysis. The first makes use of the cumulant expansion (Rahman et al., 1962)

$$\langle e^{i\vec{q} \cdot (\vec{R}(t) - \vec{R}(0))} \rangle = e^{-1/2 \langle \{\vec{q} \cdot (\vec{R}(t) - \vec{R}(0))\}^2 \rangle \pm \dots} \quad (11)$$

Neglecting terms in the exponent of Eq. 11 of order higher than q^2 , the intermediate incoherent scattering function can be written, with the exponent averaged over all directions of \vec{q} , as

$$F_{\text{inc}}(q, t) = \frac{1}{N_{\text{atom}}} \sum_{\alpha} b_{\alpha}^2 e^{-(q^2/6) \langle (\vec{R}_{\alpha}(t) - \vec{R}_{\alpha}(0))^2 \rangle}. \quad (12)$$

The elastic scattering is determined by the $t \rightarrow \infty$ limit of $F(q, t)$, i.e., from Eq. 12,

$$S_{\text{inc}}(q, \omega = 0) = \frac{1}{N_{\text{atom}}} \sum_{\alpha} b_{\alpha}^2 e^{-(q^2/6) \langle u_{\alpha}^2 \rangle}, \quad (13)$$

where $\langle u_{\alpha}^2 \rangle$ is the $t \rightarrow \infty$ mean square displacement of atom α . Eqs. 11–13 describe the so-called Gaussian approximation. This is strictly valid for atoms in ideal gases or undergoing certain types of motion, such as harmonic oscillations or damped Langevin oscillations, and is also valid for very short times or small values of q (Rahman et al., 1962; Rahman, 1963). The range of applicability of the Gaussian approximation in a protein is examined here.

Motional heterogeneity

Eq. 13 involves a sum of Gaussians. Therefore, even if the Gaussian approximation were valid for individual atoms, because of the fact that a sum of Gaussians is itself not Gaussian, $S(q, \omega)$ will not have a Gaussian form unless all the atomic mean-square displacements happen to be identical. There will therefore be a non-Gaussian contribution to the measured scattering due to motional heterogeneity, i.e., because a distribution of mean-square displacements exists in the protein. The second approximation tested here is therefore

$$\frac{1}{N_{\text{atom}}} \sum_{\alpha=1}^{N_{\text{atom}}} b_{\alpha}^2 \exp(-\langle u_{\alpha}^2 \rangle q^2/6) \approx b_{\alpha}^2 \exp(-\langle u^2 \rangle q^2/6), \quad (14)$$

where $\langle u^2 \rangle$ is the mean square displacement averaged over the atoms in the protein. The approximation in Eq. 14 is valid for $q \rightarrow 0$, in which case $\langle u^2 \rangle$ can be obtained by taking the limiting slope as $q \rightarrow 0$ in a natural log plot of $S(q, \omega = 0)$ vs. q^2 .

Timescale dependence

We also examine here the timescale dependence of the dynamical transition behavior. This is of particular interest because it was demonstrated, using elastic neutron scattering from instruments of different energy resolutions, that dynamical transition behavior of two enzymes in cryosolvent solutions is strongly time dependent (Daniel et al., 1999). The time-dependent mean square displacements, $\langle u_{\alpha}^2(t) \rangle = \langle (\vec{R}_{\alpha}(t) - \vec{R}_{\alpha}(0))^2 \rangle$, were calculated from the molecular dynamics configurations as

$$\begin{aligned} \langle u_{\alpha}^2(t) \rangle &= \langle (\vec{R}_{\alpha}(m) - \vec{R}_{\alpha}(0))^2 \rangle \\ &\approx \frac{1}{N_t - m} \sum_{k=0}^{N_t - m - 1} (\vec{R}_{\alpha}(k + m) - \vec{R}_{\alpha}(k))^2, \end{aligned} \quad (15)$$

where the steps in the trajectory are denoted by $k = 0, \dots, N_t - 1$ and N_t is the total number of timesteps. For comparison with the appropriate neutron-derived quantity, the mean square displacements are weighted by the scattering cross-sections,

$$\langle u^2(t) \rangle = \frac{1}{N_{\text{atom}}} \sum_{\alpha=1}^{N_{\text{atom}}} b_{\alpha}^2 \langle u_{\alpha}^2(t) \rangle. \quad (16)$$

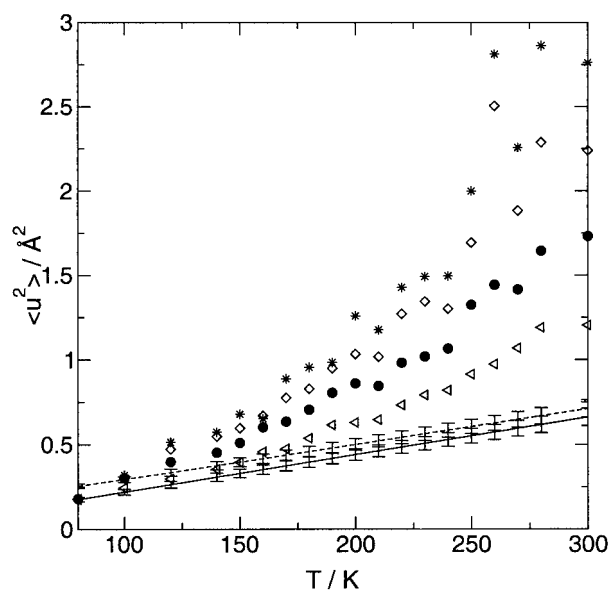


FIGURE 1 Temperature dependence of average mean square displacements, $\langle u^2(t) \rangle$, from MD simulations for times, t , of (<) 10 ps, (●) 100 ps, (◇) 500 ps, and (*) 1000 ps. Values are also shown from the normal mode analysis, in the classical (—), and quantum mechanical (---) cases. The error bars on the normal mode results are two times the standard deviation in the harmonic mean square displacements over the 20 normal mode analyses. The $\langle u^2 \rangle$ values are weighted by the atomic incoherent scattering lengths.

RESULTS

Dynamical transition

In Fig. 1, $\langle u^2(t) \rangle$ is shown at times, t , ranging from 10 to 1000 ps for each of the 19 temperatures sampled. The quantity is shown from the MD simulations, together with the quantum and classical $\langle u^2 \rangle$ from the harmonic analyses. The quantum-mechanical $\langle u^2 \rangle$ is $\sim 30\%$ larger than $\langle u^2 \rangle_{\text{class}}$ at 80 K—this difference drops to below 10% at 300 K. $\langle u^2 \rangle_{\text{qm}}$ is formally nonlinear in T (see Eq. 2). However, the deviation of $\langle u^2 \rangle_{\text{qm}}$ from linearity in Fig. 1 is clearly small, and therefore $\langle u^2 \rangle \propto T$ is a good approximation in the harmonic regime.

At 80 K, the classical MD $\langle u^2(t) \rangle$ at 10, 100, 500, and 1000 ps and the harmonic $\langle u^2 \rangle_{\text{class}}$ all coincide. The lowest frequency vibration in the harmonic analysis is 6.7 cm^{-1} , corresponding to a period of 5 ps. Therefore, the modes are adequately sampled in timescales as low as 10 ps. Consequently, at 80 K, the dynamics is entirely described by fast vibrational motions in the protein.

The MD $\langle u^2(t) \rangle$ at temperatures above 100 K is timescale dependent. Already at 150 K, one finds $\langle u^2(10 \text{ ps}) \rangle < \langle u^2(100 \text{ ps}) \rangle < \langle u^2(500 \text{ ps}) \rangle < \langle u^2(1000 \text{ ps}) \rangle$, indicating the presence of motions over a range of timescales between 10 and 1000 ps. The timescale dependence is considerably larger at higher temperatures, and at 270–300 K $\langle u^2(500 \text{ ps}) \rangle$ and $\langle u^2(1000 \text{ ps}) \rangle$ are about twice as large as $\langle u^2(10$

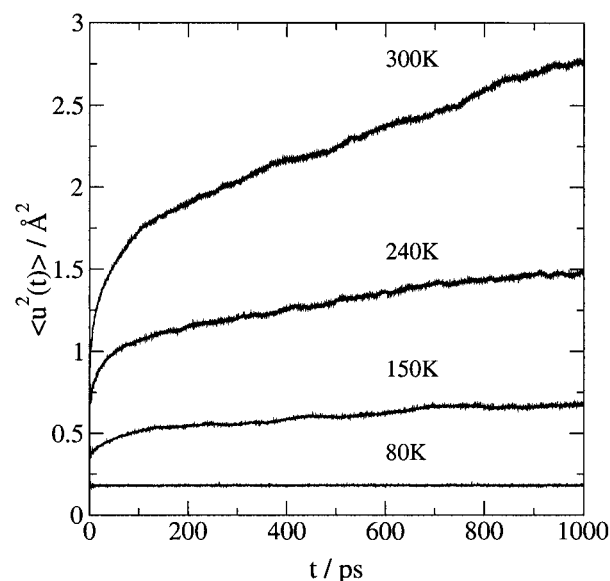


FIGURE 2 Time evolution of the mean square displacement, $\langle u^2(t) \rangle$ from MD simulation at temperatures of 80, 150, 240, and 300 K.

ps)). In Fig. 2 is shown the time evolution of $\langle u^2(t) \rangle$ at selected temperatures. This confirms the presence of significant long-timescale motion at $T \geq 150 \text{ K}$.

The MD profiles in Fig. 1 for 100 ps and longer times deviate significantly from the classical harmonic results for $T > 100 \text{ K}$, indicating the presence of anharmonic dynamics above 100 K. For these timescales, anharmonic motions contribute the major part of $\langle u^2(t) \rangle$ at 300 K. The faster, 10-ps timescale dynamics starts to deviate from harmonic behavior at a higher temperature, $T > \sim 180 \text{ K}$. That the onset of fast anharmonic dynamics is at a higher temperature than for slow dynamics is consistent with experimental results on enzyme solutions that also demonstrate a timescale dependence of $\langle u^2 \rangle$ (Daniel et al., 1999; Dunn et al., 2000). At timescales greater than 100 ps, the $\langle u^2(t) \rangle$ temperature profiles are considerably rougher at high temperatures than at shorter timescales. This reflects the presence of long-timescale (10^{-10} s) structural transitions in the protein that are incompletely sampled in the simulations. The presence of 10^{-10} -s timescale motions at high temperatures is confirmed in Fig. 2.

To our knowledge, in powdered dry protein systems, deviation from harmonic behavior has not been reported experimentally. The present results suggest that this may be due to the absence, in the experimental analyses, of a harmonic reference profile, such as is provided here by the NMA. Indeed, visual inspection suggests that the MD results in Fig. 1 should be able to be reasonably well fitted by straight lines up to 240 K, but with steeper gradients than the NMA profile. In the absence of the harmonic NMA baseline, then, the approximate linearity of the MD profiles would lead to the erroneous conclusion that little anhar-

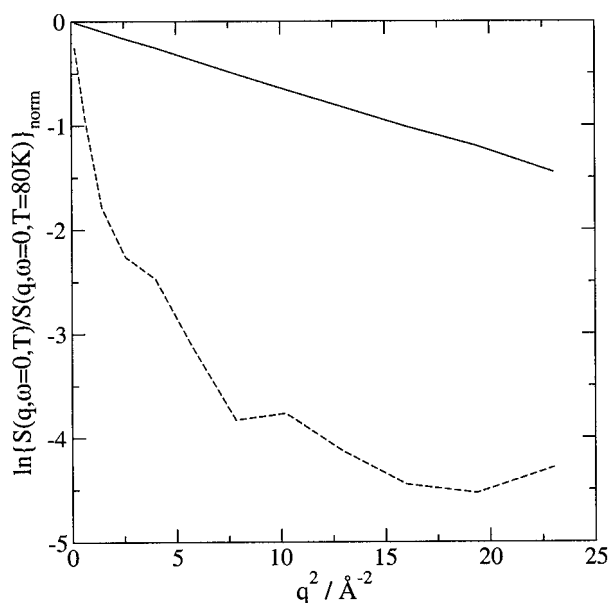


FIGURE 3 Normalized $\ln S(q, \omega = 0)$ vs. q^2 profiles for (—), the hydrogen atom with the lowest $\langle u^2 \rangle = 0.6 \text{ \AA}^2$; and (---), the hydrogen atom with the highest $\langle u^2 \rangle = 19 \text{ \AA}^2$. The elastic scattering intensity was calculated using a 20- μeV energy resolution function at 300 K.

monic behavior is present. However, as the present MD/NMA comparison shows, significant deviation from harmonic dynamics is present at temperatures as low as $\sim 100 \text{ K}$.

At higher temperatures ($> 240 \text{ K}$) a deviation from linearity is seen, especially on the longer timescales, but which is at most 10% (at 300 K). This deviation is due to increased flexibility in the loops at the C-terminal and N-terminal ends of the protein.

Gaussian approximation

The validity of the Gaussian approximation, i.e., Eqs. 12–13, is now explored by examination of the scattering calculated from individual atoms. We examine the scattering from the 300-K trajectory. At lower temperatures, the scattering may be somewhat closer to Gaussian due to reduced anharmonicity of the dynamics. $S(\vec{q}, \omega)$ was calculated for each individual atom from the 300-K MD trajectory using Eqs. 7 and 8 without invoking the Gaussian approximation. The $S(\vec{q}, \omega)$ thus obtained was convoluted with an instrumental energy resolution function (see Sect. Dynamic Structure Factor above). Two different typical energy resolutions were used, corresponding to 100 and 20 μeV full width half maximum. Subsequently, the elastic scattering intensity, $S(q, \omega = 0)$, was estimated by integrating $S(\vec{q}, \omega)$ over $\pm \Delta\omega$ where $\Delta\omega$ is the half width half maximum of the energy resolution function. Deviation from linearity in $\ln S(q, \omega = 0)$ vs. q^2 then indicates the presence of non-Gaussian scattering.

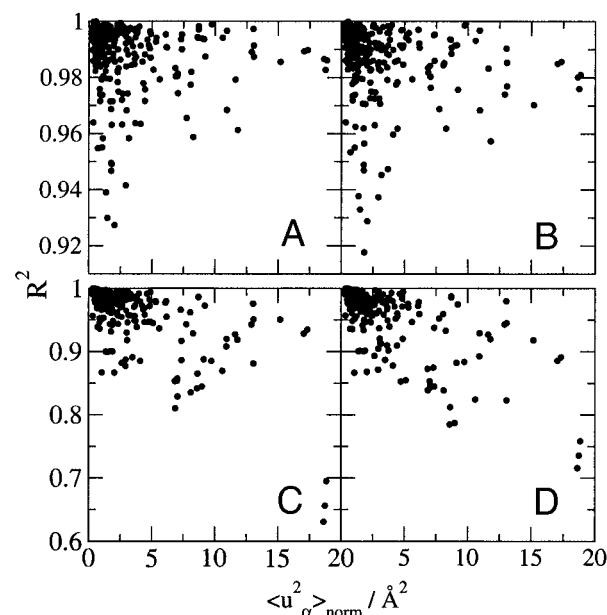


FIGURE 4 Goodness-of-fit (R^2) versus long-time $\langle u^2 \rangle$ for all hydrogen atoms at 300 K for different instrumental energy resolutions and in different q^2 ranges: (a) 100 μeV , $0.01 < q^2 < 1.44 \text{ \AA}^{-2}$; (b) 20 μeV , $0.01 < q^2 < 1.44 \text{ \AA}^{-2}$; (c) 100 μeV , $0.16 < q^2 < 23.04 \text{ \AA}^{-2}$; and (d) 20 μeV , $0.16 < q^2 < 23.04 \text{ \AA}^{-2}$. The $\langle u^2 \rangle$ are normalized to $\langle u^2 \rangle$ at 80 K. R^2 is given by $1 - \sum (y_i - y_{i,\text{fit}})^2 / \sum (y_i - \bar{y})^2$ where y_i refers to $\ln S(q, \omega = 0)$ and $y_{i,\text{fit}}$ are the fitted values of $\ln S(q, \omega = 0)$.

Plots of $\ln S(q, \omega = 0)$ vs. q^2 calculated with 20- μeV energy resolution are shown for two extreme cases in Fig. 3. Atom H α from the backbone of ARG 39 has the lowest H-atom $\langle u^2 \rangle$, of 0.6 \AA^2 , and a linear plot, demonstrating Gaussian behavior. In contrast, an H atom from the side chain $-\text{CH}_3$ in MET 52 has the largest $\langle u^2 \rangle$, of 19 \AA^2 and clearly exhibits non-Gaussian behavior over the q -range presented.

The Gaussian approximation is strictly valid for $q \rightarrow 0$. Therefore, the accuracy of the approximation will depend on the q -range examined. We now obtain an estimate of the proportion of atoms exhibiting non-Gaussian dynamics at 300 K in two different q ranges and at two different instrumental energy resolutions. The q^2 -ranges chosen are $0.01 < q^2 < 1.44 \text{ \AA}^{-2}$ (hereafter called “low- q ”) and $0.16 < q^2 < 23.04 \text{ \AA}^{-2}$ (hereafter called “high- q ”). These are similar to the ranges commonly used in obtaining $\langle u^2 \rangle$ from neutron-scattering data. For example, at the Institut Laue–Langevin, Grenoble, the low- q range is available on the instruments IN6 and IN16 and the high- q range is available on IN13.

In each of the four cases, $\langle u^2 \rangle$ was obtained by fitting a straight line to $\ln S(q, \omega = 0)$ vs. q^2 . In Fig. 4, the goodness-of-fit (R^2) for each of the 315 hydrogen atoms are shown. $R^2 = 1$ indicates a perfect fit. In the low- q range (Fig. 4, a and b), R^2 is above 0.95 for 97% of the atoms, indicating that the Gaussian approximation is valid for these atoms over this q range. For low- q , there is no clear correlation

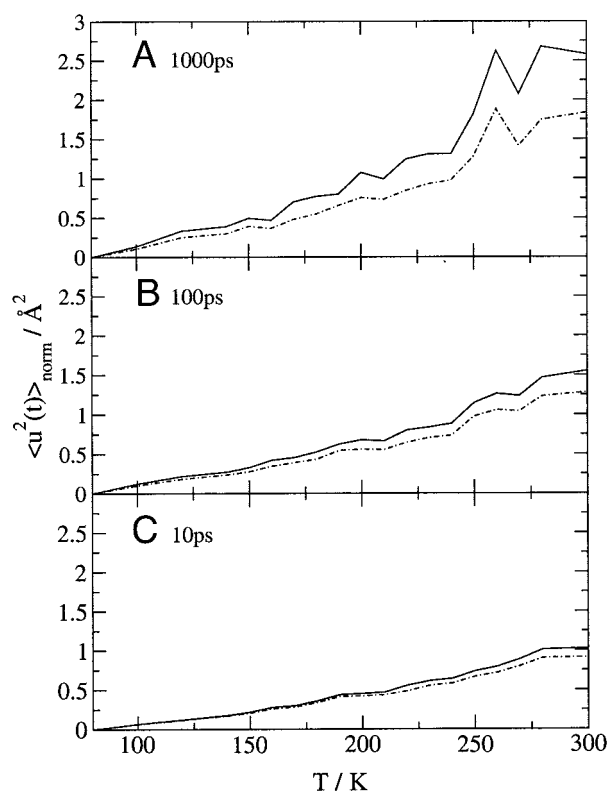


FIGURE 5 Temperature dependence of mean square displacement. The solid lines are $\langle u^2(t) \rangle$ calculated directly from the MD simulation using Eqs. 15 and 16. The dot-dashed lines are $\langle u^2 \rangle_G$ calculated from $S(q, \omega)$ over the low- q range of $0.01 < q^2 < 1.44 \text{ \AA}^{-2}$. All values are weighted by incoherent scattering lengths and have been normalized to the value at 80 K.

between R^2 and $\langle u_\alpha^2 \rangle$. In contrast, in the high- q range (Fig. 4, *c* and *d*), $\sim 20\%$ of the atoms have R^2 worse (smaller) than 0.95. There is also a correlation between R^2 and $\langle u_\alpha^2 \rangle$ in this case, the fit being poorer for atoms with large $\langle u_\alpha^2 \rangle$. For both high- and low- q , there appears to be no relation between the effectiveness of the Gaussian approximation in the examination of individual atomic motions and the instrumental resolution, or, in other words, the timescale of the motions examined. In summary, the results in Fig. 4 indicate that the Gaussian approximation is reasonable over the low- q range examined but not the high- q range, and that variation of the instrumental energy resolution between 20 and 100 \mu eV has little effect on the accuracy of the approximation.

Motional heterogeneity

We now examine the effect on $\langle u^2 \rangle$ of motional heterogeneity. In Figs. 5 and 6, $\langle u^2(t) \rangle$ is shown calculated from the MD simulations for $t = 10, 100$, and 1000 ps . Also plotted is $\langle u^2(t) \rangle_G$, obtained by inserting the individual atom $\langle u_\alpha^2(t) \rangle$ into Eq. 13, summing to obtain $S(q, \omega = 0)$ for the whole protein, and then taking the slope of $\ln S(q, \omega = 0)$ vs. q^2 .

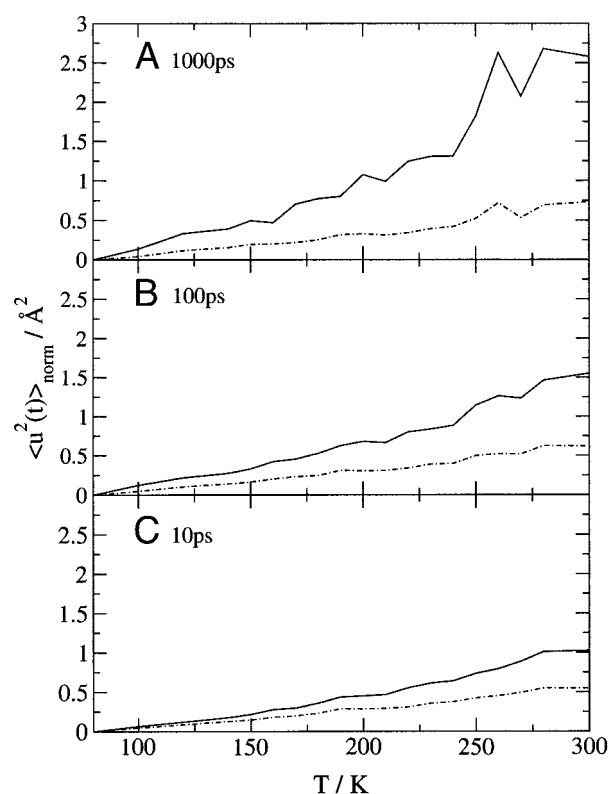


FIGURE 6 Temperature dependence of mean square displacement. The solid lines are $\langle u^2(t) \rangle$ calculated directly from the MD simulation using Eqs. 15 and 16. The dot-dashed lines are $\langle u^2 \rangle_G$ calculated from $S(q, \omega)$ over the high- q range of $0.16 < q^2 < 23.04 \text{ \AA}^{-2}$. All values are weighted by incoherent scattering lengths and have been normalized to the value at 80 K.

$\ln S(q, \omega = 0)$ vs. q^2 , thus obtained at 300 K, is shown in Fig. 7.

In Fig. 5–6, the low- q and high- q ranges are used to obtain $\langle u^2(t) \rangle_G$. It was shown in the previous section that the Gaussian approximation is valid for the low- q range, and its effect on $\langle u_\alpha^2 \rangle$ is invariant with the energy resolution (i.e., the timescale of the motions concerned). Therefore, in Fig. 5, in which the same low- q range was used, the use of the Gaussian approximation has little effect on the differences between $\langle u^2(t) \rangle_G$ and the MD simulation $\langle u^2(t) \rangle$. Rather, the differences arise from motional heterogeneity. Figure 7 shows that, at 300 K, motional heterogeneity leads to markedly non-Gaussian total scattering even when the individual atom scattering is assumed to be Gaussian. Figure 5 shows that, for the low- q range $\langle u^2(t) \rangle_G$ underestimates $\langle u^2(t) \rangle$ by $\sim 10\%$ at $t = 10 \text{ ps}$, $\sim 20\%$ at 100 ps , and $\sim 30\%$ at 1000 ps . Consequently, motional heterogeneity has a significant effect on $\langle u^2 \rangle$ that is, in addition, timescale dependent—as the timescale of the motions increase the error due to motional heterogeneity also increases.

The question now arises as to whether the timescale dependence of the effect of motional heterogeneity on the derived $\langle u^2 \rangle$ is also reflected in a timescale dependence of

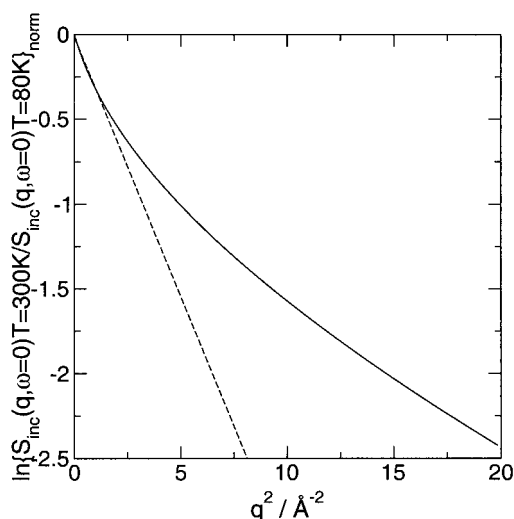


FIGURE 7 Normalized $\ln S(q, \omega = 0)$ calculated at 300 K using the Gaussian approximation (—) and the fit to $\ln S(q, \omega = 0)$ in the low- q range of $0.01 < q^2 < 1.44 \text{ \AA}^{-2}$ (---).

the distribution of $\langle u_\alpha^2(t) \rangle$ in the MD simulations. The distribution of $\langle u_\alpha^2 \rangle$ at $t = 10, 100$, and 1000 ps, is shown in Fig. 8. The range of $\langle u_\alpha^2 \rangle$ values indeed increases with timescale, from $0.3\text{--}10 \text{ \AA}^2$ at 10 ps, through $0.3\text{--}13 \text{ \AA}^2$ at 100 ps, to $0.4\text{--}19 \text{ \AA}^2$ at 1000 ps. Therefore, at longer times, $\langle u_\alpha^2 \rangle$ are more widely distributed. The distributions are approximately exponential in shape, as shown by the fitted curves in Fig. 8. The data in Fig. 8 are consistent with the conclusion drawn from Fig. 5 because the wider range of $\langle u_\alpha^2 \rangle$ at higher temperatures leads to the approximation made in Eq. 14 becoming less reliable.

In the high- q analysis (Fig. 6) the error in $\langle u^2 \rangle$ is much larger: $\sim 50\%$ at 10 ps, $\sim 60\%$ at 100 ps, and $\sim 70\%$ at 1000 ps, i.e., $\langle u^2(t) \rangle_G$ are roughly half as large as those obtained for the low- q range. This increased error arises from the cumulative effects of making the Gaussian approximation and motional heterogeneity.

Experimental data treatment of MD-derived $S(q, \omega)$

To further our practical understanding of the approximations introduced in elastic neutron-scattering data analysis, in Fig. 9, several methods for deriving the mean square displacements are compared. As reference values, the long-time ($t = 1000$ ps) MD $\langle u^2 \rangle$, calculated using Eq. 16, and the harmonic mean square displacements, $\langle u^2 \rangle_{\text{class}}$ and $\langle u^2 \rangle_{\text{qm}}$ are given. These are compared with mean square displacements obtained by analyzing $S(q, \omega)$ from the MD trajectories as if it were experimentally derived, i.e., by subjecting the MD-derived $S(q, \omega)$ to various data-analysis procedures adopted experimentally. In performing the experimental data treatments, we examine the effect of varying instru-

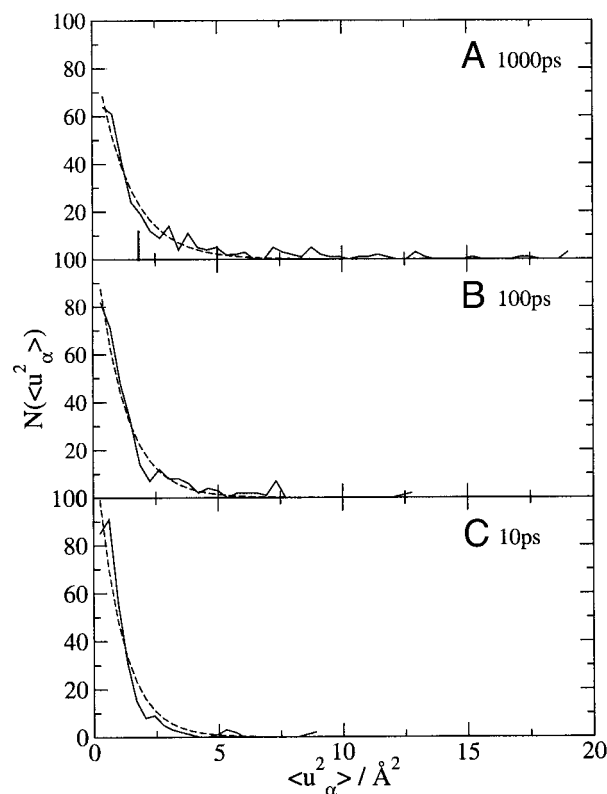


FIGURE 8 Distribution $N(\langle u_\alpha^2 \rangle)$ of $\langle u_\alpha^2 \rangle$ for hydrogen atoms at 300 K (solid lines). A function of the form $y = A \exp(-xB)$ was fitted to the distributions. The parameters A and B found from the fitting are: (a) $A = 128.7$, $B = 1.0$ for 10 ps; (b) $A = 115.3$, $B = 0.9$ for 100 ps; and (c) $A = 93.3$, $B = 0.8$ for 1000 ps. The fits to the distributions are shown as dashed lines. The vertical line in (a) indicates $\langle u^2 \rangle_G = 1.836 \text{ \AA}^2$, calculated in the low- q range of $0.01 < q^2 < 1.44 \text{ \AA}^{-2}$ at 300 K.

mental energy resolution and both effects that have been individually examined in the previous two sections, i.e., motional heterogeneity and the Gaussian approximation. The following experimental data treatments were performed:

1. $\langle u^2 \rangle_{\text{nores}}$ was obtained by calculating $S(q, \omega)$ from Eqs. 7 and 8 without convolution with an instrumental resolution function, taking the elastic peak intensity $S(q, \omega = 0)$, and fitting a straight line to $\ln S(q, \omega = 0)$ vs. q^2 between $0.01 < q^2 < 1.44 \text{ \AA}^{-2}$. This analysis corresponds to a low- q analysis that would be made experimentally on an instrument of very high energy resolution, i.e., $< 0.1 \text{ \mu eV}$. Because a low- q range is being used, the Gaussian approximation is valid, and motional heterogeneity is the only significant effect here.
2. $\langle u^2 \rangle_{\text{Elowq}}$ was calculated using the same procedure as in 1 above but $S(q, \omega)$ is convoluted with a $20\text{-}\mu\text{eV}$ full width at half maximum resolution function, and $S(q, \omega = 0)$ is consequently obtained by integrating $S(q, \omega)$ over $\pm \Delta\omega = 10 \text{ \mu eV}$. The low- q range ($0.0 < q^2 < 1.44 \text{ \AA}^{-2}$) is again used. In this treatment, motional hetero-

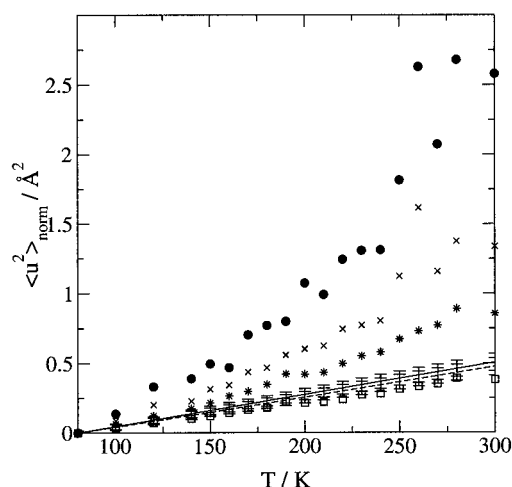


FIGURE 9 Temperature dependence of the mean square displacement for: (●) long-time MD $\langle u^2(1 \text{ ns}) \rangle$; (×) $\langle u^2 \rangle_{\text{nores}}$; (*) $\langle u^2 \rangle_{\text{Elowq}}$; (□) $\langle u^2 \rangle_{\text{Ehighq}}$; (—) $\langle u^2 \rangle_{\text{class}}$; and (---) $\langle u^2 \rangle_{\text{qm}}$. All mean square displacements are normalized with respect to the 80-K value.

geneity and the energy-resolution function (timescale dependence) will significantly affect the results, whereas the Gaussian approximation remains valid.

3. $\langle u^2 \rangle_{\text{Ehighq}}$ is calculated using the same procedure as in 2 above but using the high- q range ($0.16 < q^2 < 23.04 \text{ \AA}^{-2}$). Motional heterogeneity, the Gaussian approximation, and the effect of limited instrumental energy resolution are all expected to significantly affect the results here.

Figure 9 shows that, above $\sim 100 \text{ K}$ the MD-derived long-time $\langle u^2 \rangle$ are significantly larger than $\langle u^2 \rangle$ obtained from any of the experimental data-treatment methods. $\langle u^2 \rangle_{\text{nores}}$ is $\sim 30\%$ lower than the long-time $\langle u^2 \rangle$. The only significant approximation made in the derivation of $\langle u^2 \rangle_{\text{nores}}$ is the neglect of motional heterogeneity. The 30% reduction in $\langle u^2 \rangle$ is in accord with that found in the previous section when comparing $\langle u^2 \rangle$ and $\langle u^2 \rangle_{\text{G}}$ over the same q range. It is also consistent with the observation that $\langle u^2 \rangle_{\text{G}}$ and $\langle u^2 \rangle_{\text{nores}}$ have similar values, although they were calculated using different methods.

In $\langle u^2 \rangle_{\text{Elowq}}$, the effect of limited energy resolution is added to that of motional heterogeneity. The result is $\sim 50\%$ lower than the long-time $\langle u^2 \rangle$. Comparing $\langle u^2 \rangle_{\text{Elowq}}$ with $\langle u^2 \rangle_{\text{nores}}$, shows that the $20\text{-}\mu\text{eV}$ energy resolution decreases $\langle u^2 \rangle$ by $\sim 20\%$.

The q -range used in obtaining $\langle u^2 \rangle$ also has a large impact on the results. A high- q range introduces errors due to making the Gaussian approximation into $\langle u^2 \rangle_{\text{Ehighq}}$, along with the effects already examined, motional heterogeneity and energy-resolution function. The combination of all three effects reduces $\langle u^2 \rangle$ by $\sim 70\%$. Indeed, $\langle u^2 \rangle_{\text{Ehighq}}$ is lower than $\langle u^2 \rangle$ obtained with a harmonic model. Comparing $\langle u^2 \rangle_{\text{Ehighq}}$ with $\langle u^2 \rangle_{\text{Elowq}}$ indicates that the Gaussian approximation reduces $\langle u^2 \rangle$ by $\sim 20\%$.

The various effects examined above all reduce the values of $\langle u^2 \rangle$ obtained from elastic neutron-scattering analyses. To a first approximation, reduction of $\langle u^2 \rangle$ can be considered equivalent to reduction of the timescale at which the motions are observed. Therefore, we determined the effective timescales of the various experimental $\langle u^2 \rangle$ by determining for which value of $\langle u^2(t) \rangle$ from the simulation is closest to the $\langle u^2 \rangle$ obtained from each of the three data treatments. It was not possible to obtain a meaningful least-squares fit of $\langle u^2(t) \rangle$ to $\langle u^2 \rangle_{\text{Ehighq}}$. However, the fits for $\langle u^2 \rangle_{\text{nores}}$ and $\langle u^2 \rangle_{\text{Elowq}}$ were satisfactory (data not shown), leading to best agreement for $t = 92 \text{ ps}$ and 5 ps , respectively. This means that the effect of motional heterogeneity is equivalent to reducing the effective timescale of the motions examined by $\sim 90\%$ (92 ps compared to the MD simulation reference value of $t = 1000 \text{ ps}$), and that of motional heterogeneity combined with the $20\text{-}\mu\text{eV}$ energy resolution function decreases the effective timescale of observable motions by $\sim 99.5\%$ (5 ps compared with 1000 ps).

CONCLUSIONS

The present article examines aspects of the temperature dependence of protein dynamics and how information on this can be extracted from elastic neutron scattering. The theoretical model system examined is that of a single BPTI molecule. This is an approximation of a dry protein experimental system that neglects environmental effects such as the possible presence of protein-protein contacts in an experimental system. In the cases of dry proteins examined experimentally so far, to our knowledge, the presence of dynamical transition behavior (from harmonic to anharmonic dynamics with increasing temperature) has not yet been reported. However, the present simulations clearly show the activation of anharmonic motions on a range of timescales and at temperatures ($\sim 100\text{--}120 \text{ K}$) significantly lower than hitherto reported, also for solvated proteins. Therefore, although ample evidence exists that dynamical transition behavior is strongly coupled to solvent (see e.g., Ferrand et al., 1993; Demmel et al., 1997; Fitter et al., 1998a,b; Fitter, 1999; Vitkup et al., 2000; Réat et al., 2000) the present analysis indicates that the potential surface of an isolated protein in vacuum also contains significant anharmonicities that are sampled by the protein on the $\sim 10^{-11}\text{--}10^{-10}\text{-s}$ timescales at intriguingly low temperatures. The identification of the presence of anharmonic dynamics was made possible by the existence of a harmonic reference model. In the absence of this, as is the case experimentally, it is shown here that it is difficult to detect the presence of anharmonic dynamics in the protein.

The investigation of elastic neutron-scattering properties presented here quantifies instrumental and data-analysis effects on the basic quantity hitherto obtained, the average mean square displacement of the atoms in a protein, $\langle u^2 \rangle$. Only a representative sample of possible experimental con-

figurations and analysis parameters could be examined here. However, several findings emerge that are likely to be of general relevance. First, in the effects examined here, which are due to the use of the Gaussian approximation, the presence of motional heterogeneity and of finite instrumental energy resolution, all lead to significant underestimation of $\langle u^2 \rangle$. Motional heterogeneity, which is the presence of a distribution of mean square displacements in a protein, rather than a single average value, clearly cannot be avoided by varying instrumental conditions. Indeed, in the case of $\langle u^2 \rangle_{\text{nores}}$ calculated here, the fictitious instrument simulated has a near-perfect energy resolution (better than 0.1 μeV) and yet the motional heterogeneity effect still depresses $\langle u^2 \rangle$ by $\sim 30\%$ over the whole temperature range examined.

In contrast, the other two effects investigated, arising from the Gaussian approximation and the energy resolution, can be affected by the choice of instrument used and the analysis method. The present results suggest that the analysis of data over the range ($0.0 < q^2 < \sim 1.5 \text{ \AA}^{-2}$) avoids problems associated with the use of the Gaussian approximation. Analysis over a higher q range leads to significant errors.

The effect of instrumental energy resolution on the $\langle u^2 \rangle$ obtained is also demonstrated. In the case shown here, the use of a 20- μeV resolution function combined with the above-mentioned motional heterogeneity effect leads to reduction of the effective timescale probed to ~ 5 ps. However, varying the instrumental energy resolution can be used to advantage, because it allows motions on different timescales to be separately determined. This property was exploited recently in an analysis that demonstrated strong differences in dynamical transition behavior between 1- and 50- μeV resolution in an enzyme-cryosolvent solution (Daniel et al., 1999).

Exactly how much the various effects examined have depressed the $\langle u^2 \rangle$ obtained in experimental analyses performed so far can be estimated by comparison of the wide variety of experimental conditions hitherto used with the results presented in Fig. 9. This figure and the present work illustrate how the use of a set of atomic trajectories derived from computer simulation can allow a detailed analysis of the effects of approximations used in experimental data treatment on derived dynamical quantities.

We acknowledge the High Performance Computing Center in Karlsruhe, Germany, for time on their IBM RS/6000 SP-256. We thank Sirius Zarkhsh for calculating mean square displacements from the normal mode analyses, and Torsten Becker and Alex Tournier for useful discussions.

REFERENCES

- Angell, C. A. 1995. Formation of glasses from liquids and biopolymers. *Science*. 267:1924–1935.
- Berman, H. M., J. Westbrook, Z. Feng, G. Gilliland, T. N. Bhat, H. Weissig, I. N. Shindyalov, and P. E. Bourne. 2000. The protein data bank. *Nucleic Acids Res.* 28:235–242.
- Brooks, B. R., R. E. Bruccoleri, B. D. Olafson, D. J. States, S. Swaminathan, and M. Karplus. 1983. CHARMM. *J. Comput. Chem.* 4:187–217.
- Cordone, L., M. Ferrand, E. Vitrano, and G. Zaccai. 1999. Harmonic behavior of trehalose-coated carbon-monoxymyoglobin at high temperature. *Biophys. J.* 76:1043–1047.
- Cordone, L., P. Galajda, E. Vitrano, A. Gassmann, A. Ostermann, and F. Parak. 1998. A reduction of protein specific motions in co-ligated myoglobin embedded in a trehalose glass. *Eur. Biophys. J.* 27:173–176.
- Daniel, R. M., J. L. Finney, V. Réat, R. Dunn, M. Ferrand, and J. C. Smith. 1999. Enzyme dynamics and activity: time-scale dependence of dynamical transitions in glutamate dehydrogenase solution. *Biophys. J.* 77:2184–2190.
- Daniel, R. M., J. C. Smith, M. Ferrand, S. Héry, R. Dunn, and J. L. Finney. 1998. Enzyme activity below the dynamical transition at 220 K. *Biophys. J.* 75:2504–2507.
- Demmel, F., W. Doster, W. Petry, and A. Schulte. 1997. Vibrational frequency shifts as a probe of hydrogen bonds: thermal expansion and glass transition of myoglobin in mixed solvents. *Eur. Biophys. J.* 26:327–335.
- Ding, X., B. Rasmussen, G. A. Petesko, and D. Ringe. 1994. Direct structural observation of an acyl-enzyme intermediate in the hydrolysis of an ester substrate by elastase. *Biochemistry*. 33:9285–9293.
- Doster, W., S. Cusack, and W. Petry. 1989. Dynamical transition of myoglobin revealed by inelastic neutron scattering. *Nature*. 337:754–756.
- Dunn, R. V., V. Réat, J. Finney, M. Ferrand, J. C. Smith, and R. M. Daniel. 2000. Enzyme activity and dynamics: xylanase activity in the absence of fast anharmonic dynamics. *Biochem. J.* 346:355–358.
- Elber, R., and M. Karplus. 1987. Multiple conformation states of proteins: a molecular dynamics analysis of myoglobin. *Science*. 235:318–321.
- Ferrand, M., A. J. Dianoux, W. Petry, and G. Zaccai. 1993. Thermal motions and function of bacteriorhodopsin in purple membranes: effects of temperature and hydration studied by neutron scattering. *Proc. Natl. Acad. Sci. U.S.A.* 90:9668–9672.
- Fitter, J. 1999. The temperature dependence of internal molecular motions in hydrated and dry α -amylase: the role of hydration water in the dynamical transition of proteins. *Biophys. J.* 76:1034–1042.
- Fitter, J., O. P. Ernst, T. Hauss, R. E. Lechner, K. P. Hoffmann, and N. A. Dencher. 1998a. Molecular motions and hydration of purple membranes and disk membranes studied by neutron scattering. *Eur. Biophys. J.* 27:638–645.
- Fitter, J., R. E. Lechner, and N. A. Dencher. 1997. Picosecond molecular motions in bacteriorhodopsin from neutron scattering. *Biophys. J.* 73:2126–2137.
- Fitter, J., S. A. W. Verclas, R. E. Lechner, H. Seelert, and N. A. Dencher. 1998b. Function and picosecond dynamics of bacteriorhodopsin in purple membrane at different lipidation and hydration. *FEBS Lett.* 433:321–325.
- Frauenfelder, H., S. G. Sligar, and P. G. Wolynes. 1991. The energy landscapes and motions of proteins. *Science*. 254:1598–1603.
- Jorgensen, W. L., J. Chandrasekhar, J. D. Madura, R. W. Impey, and M. L. Klein. 1983. Comparison of simple potential functions for simulating liquid water. *J. Chem. Phys.* 79:926–935.
- Karplus, M., and G. A. Petsko. 1990. Molecular dynamics simulations in biology. *Nature*. 347:631–639.
- Knapp, E. W., S. F. Fischer, and F. Parak. 1982. Protein dynamics from Mössbauer. *J. Phys. Chem.* 86:5042–5047.
- Kneller, G. R., V. Keiner, M. Kneller, and M. Schiller. 1995. nMOLDYN: a program package for a neutron scattering oriented analysis of molecular dynamics simulations. *Comp. Phys. Commun.* 91:191–214.
- Kneller, G. R., and J. C. Smith. 1994. Liquid-like side-chain dynamics in myoglobin. *J. Mol. Biol.* 242:181–185.
- Lamy, A. V., M. Souaille, and J. C. Smith. 1996. Simulation evidence for experimentally detectable low-temperature vibrational inhomogeneity in a globular protein. *Biopolymers*. 39:471–478.
- Lehnert, U., V. Réat, M. Weik, G. Zaccai, and C. Pfister. 1998. Thermal motions in bacteriorhodopsin at different hydration levels studied by

- neutron scattering: correlation with kinetics and light-induced conformational changes. *Biophys. J.* 75:1945–1952.
- Lovesey, S. W. 1984. *Theory of Neutron Scattering from Condensed Matter*. Clarendon Press, Oxford, U.K.
- Mackerell, A. D., D. Bashford, M. Bellot, J. R. Dunbrack, R. L. Evenseck, M. J. Field, S. Fischer, J. Gao, H. Guo, S. Ha, D. Joseph, L. Kuchnir, K. Kuczera, F. T. K. Lau, C. Mattos, S. Michnick, T. Ngo, D. T. Nguyen, B. Prodhom, I. W. E. Reiher, B. Roux, M. Schlenkrich, J. C. Smith, R. Stote, J. Straub, M. Watanabe, J. Wiorkiewicz-Kuczera, J. Yin, and M. Karplus. 1998. All-atom empirical potential for molecular modelling and dynamics studies of proteins. *J. Phys. Chem. B.* 102:3586–3616.
- Ostermann, A., R. Waschipky, F. G. Parak, and G. U. Nienhaus. 2000. Ligand binding and conformational motions in myoglobin. *Nature*. 404:205–208.
- Parak, F., E. N. Frolov, A. A. Kononenko, R. L. Mössbauer, V. I. Goldanskii, and A. B. Rubin. 1980. Evidence for a correlation between the photoinduced electron transfer and dynamic properties of the chromatophore membranes from *Rhodospirillum rubrum*. *FEBS Lett.* 117: 368–372.
- Parak, F., and E. W. Knapp. 1984. A consistent picture of protein dynamics. *Proc. Natl. Acad. Sci. U.S.A.* 81:7088–7092.
- Parkin, S., B. Rupp, and H. Hope. 1996. Structure of bovine pancreatic trypsin inhibitor at 125K: definition of carboxyl-terminal residues Gly57 and Ala58. *Crystallogr. D. Biol. Crystallogr.* 52:18–29.
- Rahman, A. 1963. Intermediate scattering function in slow neutron scattering. *Phys. Rev.* 130:1334–1336.
- Rahman, A., K. S. Singwi, and A. Sjölander. 1962. Theory of slow neutron scattering by liquids. I. *Phys. Rev.* 126:986–996.
- Rasmussen, B. F., A. M. Stock, D. Ringe, and G. A. Petsko. 1992. Crystalline ribonuclease A loses function below the dynamical transition at 220K. *Nature*. 357:423–424.
- Réat, V., R. Dunn, M. Ferrand, J. L. Finney, R. M. Daniel, and J. C. Smith. 2000. Solvent dependence of dynamic transitions in protein solutions. *Proc. Natl. Acad. Sci. U.S.A.* 97:9961–9966.
- Ryckaert, J. P., G. Ciccotti, and H. J. C. Berendsen. 1977. Numerical integration of the cartesian equations of motion of a system with constraints: molecular dynamics of *n*-alkanes (SHAKE). *J. Comput. Phys.* 23:327–341.
- Smith, J. C. 1991. Protein dynamics: comparison of simulations with inelastic neutron scattering experiments. *Quart. Rev. Biophys.* 24: 227–291.
- Smith, J. C. 2000. Inelastic and quasielastic neutron scattering: complementarity with biomolecular simulation. In *Structure and Dynamics of Biomolecules: Neutron Synchrotron Radiation for Condensed Matter Studies*. Oxford University Press, Oxford, U.K. 161–180.
- Smith, J. C., K. Kuczera, and M. Karplus. 1990. Temperature-dependence of myoglobin dynamics: neutron spectra calculated from molecular dynamics simulations of myoglobin. *Proc. Natl. Acad. Sci. U.S.A.* 87: 1601–1605.
- Steinbach, P. J., and B. R. Brooks. 1994. New spherical-cutoff methods for long-range forces in macromolecular simulation. *J. Comp. Chem.* 15: 667–683.
- Vitkup, D., D. Ringe, G. A. Petsko, and M. Karplus. 2000. Solvent mobility and the protein glass transition. *Nature Struct. Biol.* 7:34–38.
- Zaccai, G. 2000. Moist and soft, dry and stiff: a review of neutron experiments on hydrations-dynamics-activity relations in the purple membrane of *Halobacterium salinarum*. *Biophys. Chem.* 86:249–257.